AGU PUBLICATIONS

Space Weather

RESEARCH ARTICLE
10.1002/2016SW001486

Special Section:
Sun to Earth: Heliospheric Remote Sensing Observations Applicable to Space Weather

Key Points:
- COSMIC derived electron densities are used to estimate the Pedersen conductivity at high latitudes
- Solar radiation and geomagnetic activity are found to influence the ionospheric Pedersen conductance in different ways
- *E* and *F* region Pedersen conductances and their ratio on the nightside have a larger difference in the postmidnight sector between the two hemispheres

Correspondence to:
C. Sheng,
csheng@ucar.edu

Citation:
Sheng, C., Y. Deng, Y. Lu, and X. Yue (2017), Dependence of Pedersen conductance in the *E* and *F* regions and their ratio on the solar and geomagnetic activities, *Space Weather*, *15*, doi:10.1002/2016SW001486.

Received 1 AUG 2016
Accepted 13 FEB 2017
Accepted article online 17 FEB 2017

Dependence of Pedersen conductance in the *E* and *F* regions and their ratio on the solar and geomagnetic activities

Cheng Sheng[1], Yue Deng[2], Yang Lu[2], and Xinan Yue[3]

[1]High Altitude Observatory, National Center for Atmospheric Research, Boulder, Colorado, USA, [2]Department of Physics, University of Texas at Arlington, Arlington, Texas, USA, [3]Institute of Geology and Geophysics, Chinese Academy of Sciences, Beijing, China

Abstract Ionospheric conductivity plays an important role in the magnetosphere-ionosphere coupling. The altitudinal distribution of Pedersen conductivity gives us a rough idea about the altitudinal distribution of Joule heating at high latitudes, which is of great significance regarding the response of upper atmosphere to geomagnetic energy inputs. Based on the electron density profiles derived from the Constellation Observing System for Meteorology, Ionosphere, and Climate measurements during 2009–2014, Pedersen conductivity has been estimated. A climatologic study of the height-integrated Pedersen conductivity in both *E* (100–150 km) and *F* (150–600 km) regions, i.e., Σ_{PE} and Σ_{PF}, and their ratio ($\gamma_P = \Sigma_{PE}/\Sigma_{PF}$) under different solar and geomagnetic conditions has been conducted. Both Σ_{PE} and Σ_{PF} increase with $F_{10.7}$ and *Ap* indices. Their ratio is smaller at higher solar flux but larger under more disturbed geomagnetic conditions. Meanwhile, an interhemispheric asymmetry has been identified in the *Ap* and $F_{10.7}$ dependencies of γ_P, which also varies with local time. These results will help to improve our understanding of the variations of the altitudinal energy distribution under different solar and geomagnetic conditions and the interhemispheric asymmetry of the high-latitude electrodynamics.

1. Introduction

Understanding and being able to predict the ionospheric and thermospheric response to geomagnetic energy inputs is of great importance in the context of space weather. During geomagnetically disturbed times, magnetospheric energy, in the forms of Joule heating and particle precipitation, flows into the coupled ionosphere-thermosphere (IT) system and generates a series of disturbances [*Buonsanto*, 1999; *Richmond and Lu*, 2000; *Danilov and Lastovicka*, 2001]. Such disturbances have strong, adverse impacts on low-Earth orbit satellite operations, Global Position System (GPS) based navigations, and power grids [*Scherer et al.*, 2005; *Moldwin*, 2008]. One of the key factors controlling the energy transfer between the magnetosphere and the IT system is ionospheric conductivity, which directly determines the Joule heating rate [*Thayer et al.*, 1995; *Strangeway*, 2012]. However, not like some other ionospheric parameters, conductivity cannot be measured directly and is usually inferred from radar measurements of ionospheric electron density [*Brekke et al.*, 1974; *Robinson and Vondrak*, 1984; *Moen and Brekke*, 1993] or satellite measurements of particle precipitation at the topside ionosphere [*Spiro et al.*, 1982; *Robinson et al.*, 1987; *McGranaghan et al.*, 2015, 2016].

The Constellation Observing System for Meteorology, Ionosphere, and Climate (COSMIC) is a joint Taiwan-US mission, consisting six identical microsatellites [*Rocken et al.*, 2000]. With the radio occultation technique, COSMIC has been providing continuous, global measurements of ionospheric total electron density (TEC), which can be further inverted to electron density profiles (EDPs) by applying an Abel inversion with the assumption of spherical symmetry of the ionosphere [*Hajj et al.*, 2000; *Wu et al.*, 2005; *Schreiner et al.*, 2007; *Lei et al.*, 2007; *Anthes et al.*, 2008; *Pedatella et al.*, 2015]. TEC and EDPs from COSMIC measurements have been widely used in low- and middle-latitude ionospheric studies [*Burns et al.*, 2008; *Zeng et al.*, 2008; *Luan et al.*, 2008; *He et al.*, 2009; *Yue et al.*, 2010a, 2010b, 2012; *Pedatella et al.*, 2014]. *Yue et al.* [2013] initiated a data quality investigation for electron densities derived from COSMIC measurements at high latitudes. Following that, *Sheng et al.* [2014] demonstrated the feasibility of utilizing the EDPs from COSMIC measurements to estimate the ionospheric conductivity on a global scale. The height-integrated conductivity in both *E* and *F* regions, i.e., Σ_{PE} and Σ_{PF}, and their ratio ($\gamma_P = \Sigma_{PE}/\Sigma_{PF}$) have been compared with the Thermosphere Ionosphere Electrodynamics General Circulation Model (TIEGCM) outputs, and it is found that the simulated ratio is relatively larger in the auroral zone, which indicates the energy input in the high-latitude *F* region may be underestimated in the model. Besides COSMIC, DMSP satellites also provide a decent coverage of particle precipitation measurements, based on which ionospheric conductance maps at high latitudes can be constructed [*McGranaghan et al.*, 2015].

Solar radiation is the major source for ionospheric conductivity, and the relationship between them has been determined theoretically [*Rasmussen et al.*, 1988] and observationally [*Brekke et al.*, 1974; *Robinson and Vondrak*, 1984; *Moen and Brekke*, 1993]. At high latitudes, particle precipitation becomes another important source, especially during disturbed times. Many efforts have been devoted to estimate the ionospheric conductivity due to particle precipitation [*Vickrey et al.*, 1981; *Spiro et al.*, 1982; *Fuller-Rowell and Evans*, 1987; *Hardy et al.*, 1987; *Robinson et al.*, 1987; *Kaeppler et al.*, 2015; *McGranaghan et al.*, 2015, 2016]. Therefore, both solar radiation and geomagnetic activity can affect the ionospheric conductivity, but it is not clear how the altitudinal distribution of the conductivity changes under different conditions. In this paper, we present the *Ap* and $F_{10.7}$ dependencies of Pedersen conductance in both *E* and *F* regions, i.e., Σ_{PE} and Σ_{PF}, and their ratio utilizing the EDPs from COSMIC measurements. It is found that both Σ_{PE} and Σ_{PF} increase with *Ap* and $F_{10.7}$ indices. Their ratio is larger when the geomagnetic activity is stronger, but smaller when the solar flux is higher.

2. Methodology

COSMIC has been continuously providing 1000+ EDPs per day since launch. COSMIC EDPs in the altitude range of 100–600 km from 2009 to 2014 have been used in this study. For each positive data point of electron density, the corresponding Pedersen conductivity was calculated based on the formula in *Evans et al.* [1977],

$$\sigma_P = \frac{en_e}{B}\left\{\sum_i C_i\left[\frac{\nu_{in}/\omega_i}{1+(\nu_{in}^2/\omega_i^2)}\right] + \frac{\nu_e/\omega_e}{1+(\nu_e^2/\omega_e^2)}\right\}, \tag{1}$$

where n_e is the electron density, B is the magnetic field, C_i is the relative concentration of ion species i, ν_{in} is the collision frequency between an ion of species i and neutral particles, ω_i is the ion gyrofrequency, ν_e is the sum of electron-ion and electron-neutral collision frequencies, and ω_e is the electron gyrofrequency. Further details regarding the conductivity calculation from COSMIC EDPs can be found in *Sheng et al.* [2014]. The calculated Pedersen conductivity was binned to a three-dimensional grid, with the grid size of 2.5° in latitude, 1 h in MLT, and 5 km in altitude. For each grid, the average conductivity was solved after including all the electron densities derived from COSMIC measurements. The conductivity was then integrated along altitude to get height-integrated Pedersen conductivity in the *E* (100–150 km) and *F* (150–600 km) regions, i.e., Σ_{PE} and Σ_{PF}. At this step, two-dimensional maps (longitude×latitude) of Σ_{PE} and Σ_{PF} were generated, from which the distribution of the ratio between Σ_{PE} and Σ_{PF} (γ_P) can be obtained.

The dependencies of Σ_{PE}, Σ_{PF}, and their ratio γ_P (Σ_{PE}/Σ_{PF}) on the geomagnetic activity and solar radiation are investigated in this paper. The geomagnetic activity is divided into three levels, with $Ap < 15$, $15 < Ap < 80$, and $Ap > 80$. The solar radiation is also divided into three levels, with $F_{10.7} < 100$, $100 < F_{10.7} < 150$, and $F_{10.7} > 150$. Figure 1 shows the *Ap* and $F_{10.7}$ indices from 2009 to 2014. The two horizontal dashed lines in the *Ap* plot show $Ap = 15$ and $Ap = 80$, respectively. The two in the $F_{10.7}$ plot show $F_{10.7} = 100$ and $F_{10.7} = 150$, respectively. During this period, 91.5% of the time the *Ap* index was smaller than 15, 8.2% of the time it was between 15 and 80, and 0.3% of the time it was larger than 80. For the $F_{10.7}$ index, 43.3% of the time it was smaller than 100, 45.4% of the time it was between 100 and 150, and 11.3% of the time it was larger than 150.

3. Results and Discussion

3.1. Dependence of Height-Integrated Pedersen Conductivity on the *Ap* Index

Solar extreme ultraviolet (EUV) radiation and particle precipitation are the two major sources for the ionization and conductivity in the high-latitude ionosphere. Considerable effort has been made to estimate the conductivity produced by solar EUV radiation [*Rasmussen et al.*, 1988; *Robinson and Vondrak*, 1984; *Moen and Brekke*, 1990]. The contribution from particle precipitation has also been estimated in many studies [*Spiro et al.*, 1982; *Hardy et al.*, 1987; *Robinson et al.*, 1987; *Fuller-Rowell and Evans*, 1987; *McGranaghan et al.*, 2015]. In *Robinson et al.* [1987], the height-integrated Hall and Pedersen conductivities are related to the average energy and energy flux of precipitating electrons. In this section, the dependencies of Σ_{PE}, Σ_{PF}, and the ratio γ_P on the *Ap* index are examined. The *Ap* index, which is an indicator of geomagnetic activity level, can also be used as a proxy for particle precipitation. The larger the *Ap* index is, the stronger the particle precipitation and the conductance are expected.

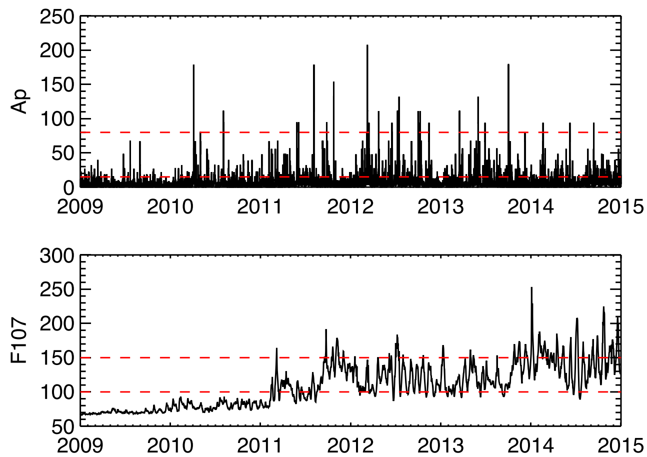

Figure 1. *Ap* and $F_{10.7}$ indices during 2009–2014. The two red dashed lines in the *Ap* plot mark $Ap = 15$ and $Ap = 80$, respectively. The two in the $F_{10.7}$ plot mark $F_{10.7} = 100$ and $F_{10.7} = 150$, respectively.

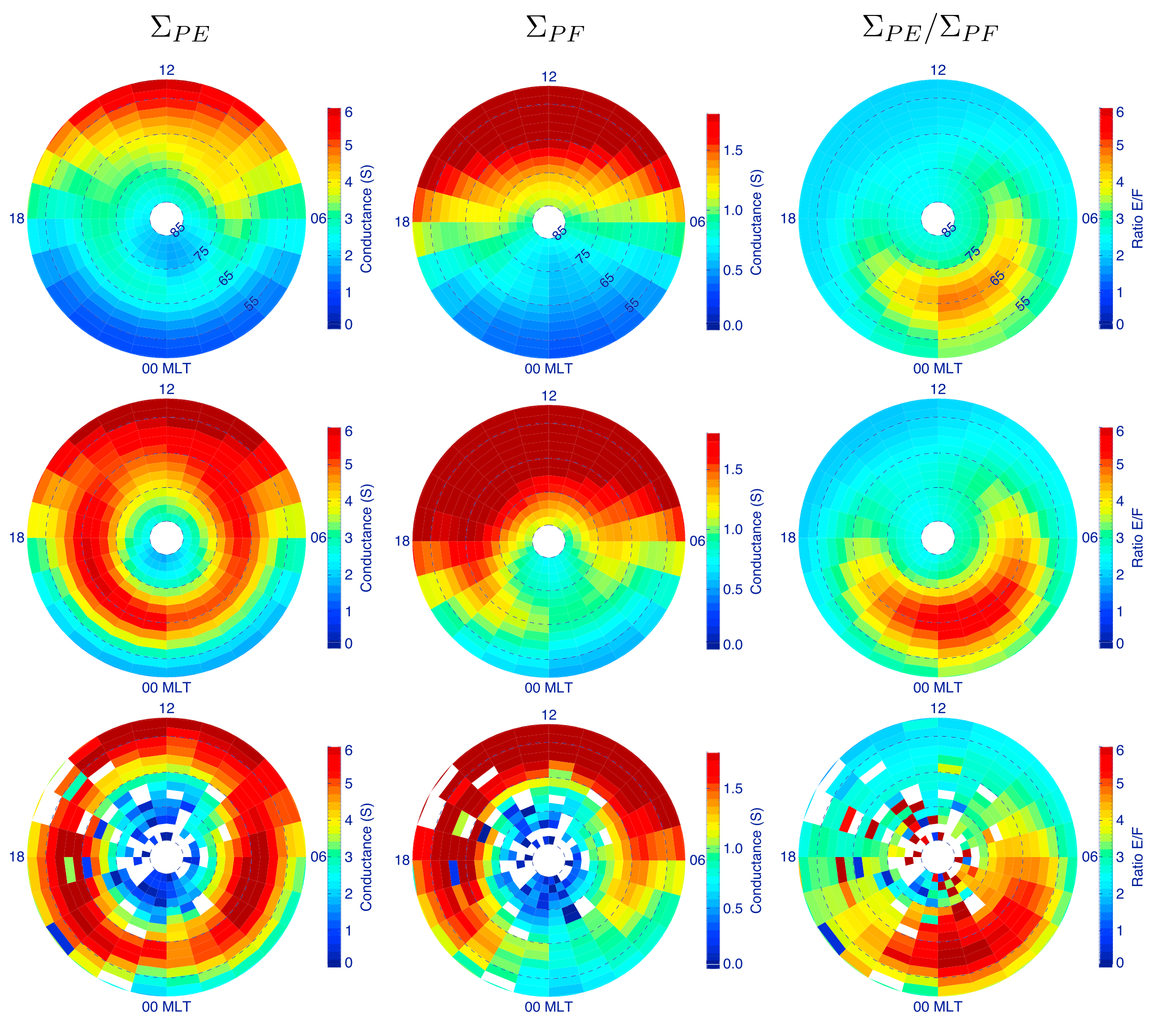

Figure 2. Pedersen conductance in the (left column) *E* region (Σ_{PE}), in the (middle column) *F* region (Σ_{PF}), and (right column) their ratio (Σ_{PE}/Σ_{PF}) under (top row) quiet ($Ap < 15$), (middle row) moderate ($15 < Ap < 80$), and (bottom row) severe ($Ap > 80$) geomagnetic conditions in the Northern Hemisphere. Magnetic coordinates are used. The dashed rings label the magnetic latitudes of 55°, 65°, 75°, and 85°, respectively. Each column shares the same color bar.

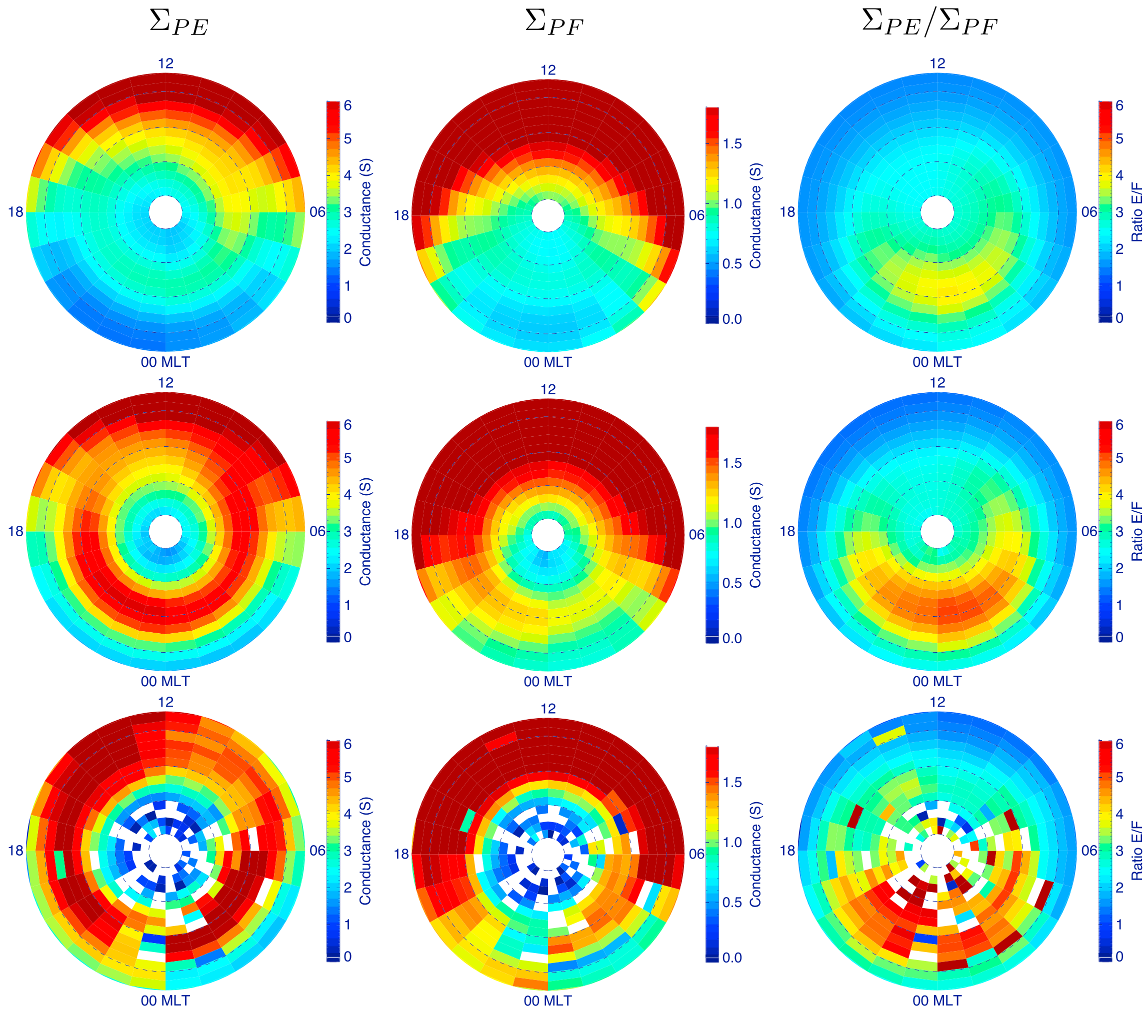

Figure 3. Same as Figure 2 but in the Southern Hemisphere.

Figure 2 shows Σ_{PE} (left column), Σ_{PF} (middle column) and their ratio γ_P (Σ_{PE}/Σ_{PF}, right column) in the Northern Hemisphere under quiet ($Ap < 15$, first row), moderate ($15 < Ap < 80$, second row) and severe ($Ap > 80$, third row) geomagnetic conditions. COSMIC-derived electron densities from 2009 to 2014 have been utilized to generate these figures. Magnetic Apex coordinates are applied, and the dashed rings label the magnetic latitudes of 55°, 65°, 75° and 85°, respectively. We will focus on the results under quiet and moderate geomagnetic conditions, since the data coverage is poor under severe conditions.

Σ_{PE} maximizes on the dayside for all conditions, due to the strong ionization caused by the EUV radiation. Σ_{PE} also has a localized peak in the nightside auroral region, which results from the auroral particle precipitation. The localized peak on the nightside under moderate conditions is larger than that under quiet conditions, changing from ~2–3 S to ~5–6 S. It is reasonable since auroral particle precipitation is more intense when geomagnetic activity is stronger. Furthermore, the nighttime peak under moderate conditions is comparable to the daytime peak, which demonstrates the significance of the contribution of auroral particle precipitation to the total conductance. Σ_{PF} also maximizes on the dayside as Σ_{PE}. During quiet time, Σ_{PF} on the nightside is relatively low and in the auroral zone it is ~0.5 S. Under moderate conditions, the magnitude increases to ~1.0 S, which indicates a considerable increase of electron density at *F* region altitudes caused by particle precipitation, especially by soft particles [*Fang et al.*, 2008; *Millward et al.*, 1999]. It is also found that under moderate conditions, Σ_{PF} in the premidnight sector is relatively larger than that in the postmidnight sector. As for the ratio γ_P (Σ_{PE}/Σ_{PF}), it maximizes on the nightside in the auroral zone under all conditions. Although Σ_{PF} does increase on the nightside from quiet to moderate conditions, Σ_{PE} increases a lot more since most of the magnetospheric energy is dissipated in the auroral *E* region. Moreover, the maximum ratio γ_P under

10.1002/2016SW001486

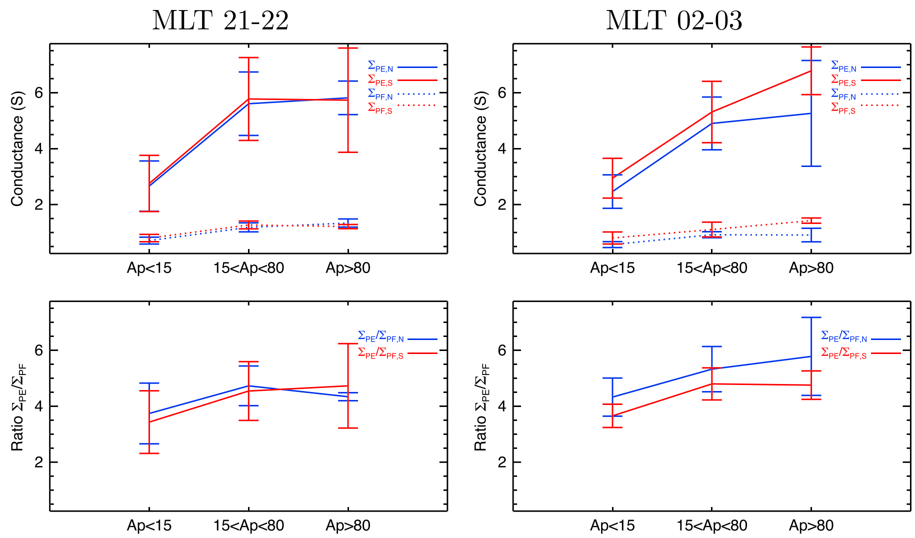

Figure 4. Comparisons of Σ_{PE}, Σ_{PF}, and their ratio (Σ_{PE}/Σ_{PF}) between the two hemispheres at (left column) MLT = 21–22 and (right column) MLT = 02–03 under different geomagnetic conditions. For each local time, the location with maximum Σ_{PE} is selected to ensure the comparisons in the auroral zone. Blue lines show for the Northern Hemisphere, and red lines show for the Southern Hemisphere. In the (top row) conductance plots, solid lines plot Σ_{PE} and dashed lines plot Σ_{PF}. Error bars represent standard deviation.

moderate conditions (~5.5) is larger than that under quiet conditions (~4.7), and the region with large ratio expands, which is likely related to the expansion of the auroral zone during active times. It is also interesting to notice that γ_P is slightly larger in the postmidnight sector than in the premidnight sector, which calls for further investigation.

Figure 3 is the same as Figure 2 except for the Southern Hemisphere. The two hemispheres share very similar features as mentioned above, but some differences can be easily identified, such as slightly larger conductance and smaller ratio γ_P under all conditions in the Southern Hemisphere. *Sheng et al.* [2014] have identified an interhemispheric asymmetry, in which the seasonal variation of the maximum ratio in the Southern Hemisphere is larger than that in the Northern Hemisphere. Here we further investigate the local time dependence of the asymmetry. Two local times have been chosen, one in the premidnight sector (21–22 MLT), and the other in the postmidnight sector (02–03 MLT). As shown in Figures 2 and 3, the maximum ratio is not necessarily coincident with the maximum Σ_{PE}. Therefore, instead of directly comparing the maximum ratio, the locations with maximum Σ_{PE} in each local time sector have been selected first to focus on the comparison in the auroral zone. Σ_{PE}, Σ_{PF}, and γ_P at those locations are then plotted out together for comparison as shown in Figure 4. The comparison for the premidnight sector is shown on the left, and the postmidnight sector on the right. Σ_{PE}, Σ_{PF}, and γ_P show a relative standard deviation of 10%–30% as indicated by the error bars. Ionospheric conductance change with solar and geomagnetic activities and may also have longitudinal, seasonal, and other dependency. These factors contribute to the standard deviation, in addition to the observational uncertainty. In the premidnight sector, Σ_{PE} and Σ_{PF} are very symmetric between the two hemispheres, and thus γ_P is very close. However, in the postmidnight sector, both Σ_{PE} and Σ_{PF} are slightly larger in the Southern Hemisphere, which may result from the unequal solar radiation in the auroral zone between the two hemispheres due to the displacement between the geomagnetic and geographic poles. γ_P is actually larger in the Northern Hemisphere in the postmidnight sector. The difference of the ratio between the two hemispheres is larger in the postmidnight sector than in the premidnight sector, which implies the local time dependence of interhemispheric asymmetry. We suspect that not only solar radiation but also auroral activity are different in the auroral zone between the two hemispheres. *Newell et al.* [2009] showed that the discrete aurora peaks in the premidnight sector and the diffuse aurora distributes from the premidnight sector to the early morning sector. Therefore, the asymmetry found in this study implies that the diffuse aurora intensities may be different in the two hemispheres.

Due to the limitation of available data, the solar flux effect was not separated when investigating the *Ap* dependency of Σ_{PE}, Σ_{PF}, and γ_P. It can be seen from Figure 1 that the *Ap* index was more likely to be larger than

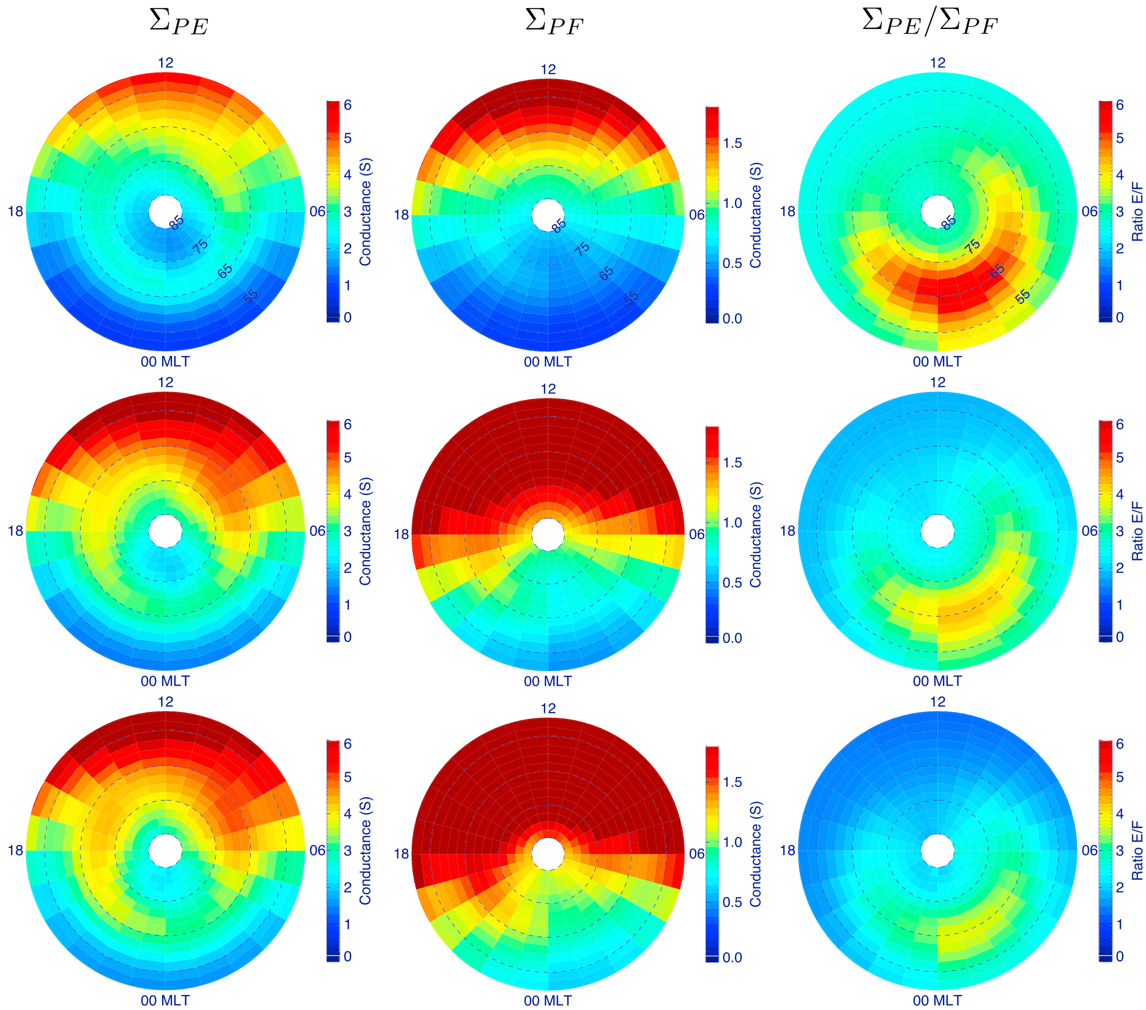

Figure 5. (left column) Σ_{PE}, (middle column) Σ_{PF}, and (right column) their ratio (Σ_{PE}/Σ_{PF}) under different levels of solar radiation, (top row) $F_{10.7} < 100$, (middle row) $100 < F_{10.7} < 150$, and (bottom row) $F_{10.7} > 150$ in the Northern Hemisphere.

15 from 2011 to 2015 when the $F_{10.7}$ was relatively larger. As we calculated the average $F_{10.7}$ and *Ap* indices for each longitude-latitude bin, the average $F_{10.7}$ index rises from ~95 to ~110 at most bins when the geomagnetic condition changes from quiet ($Ap < 15$) to moderate ($15 < Ap < 80$). Meanwhile, the average *Ap* index jumps from ~4.5 to ~29. Therefore, the influence of change in solar flux should be secondary compared with that of change in geomagnetic activity.

3.2. Dependence of Height-Integrated Pedersen Conductivity on the $F_{10.7}$ Index

Ionospheric conductivity at high latitudes is also strongly influenced by solar radiation. Analytic relationship between ionospheric conductance and $F_{10.7}$ index has been examined both theoretically and observationally in previous studies [*Robinson and Vondrak*, 1984; *Rasmussen et al.*, 1988; *Moen and Brekke*, 1993]. All these studies suggested an increase of the ionospheric conductance with increasing $F_{10.7}$. Figure 5 shows the variation of Σ_{PE} and Σ_{PF} with solar radiation in the Northern Hemisphere derived from COSMIC observations. Only data under quiet geomagnetic conditions ($Ap < 15$) are considered to minimally exclude the influence of geomagnetic activity. In Figure 5, first row shows the results for $F_{10.7} < 100$, the second row for $100 < F_{10.7} < 150$, and the last row for $F_{10.7} > 150$. In Figure 5 (top to bottom), both Σ_{PE} and Σ_{PF} show an increase with the $F_{10.7}$ index. For example, the magnitudes of Σ_{PE} at noon and midnight at 65°N increase from 3.9 S to 5.0 S and 2.4 S to 3.2 S, respectively, and the percentage increase are close to 25% and 35%, respectively. Meanwhile, the magnitudes of Σ_{PF} increase from 1.5 S to 3.4 S and 0.4 S to 0.9 S, respectively, which are more than 100% increase. It also shows that the region with larger conductance expands to higher latitudes when solar activity is stronger. The variation of the ratio is shown in Figure 5 (right column). The ratio again maximizes in the nighttime

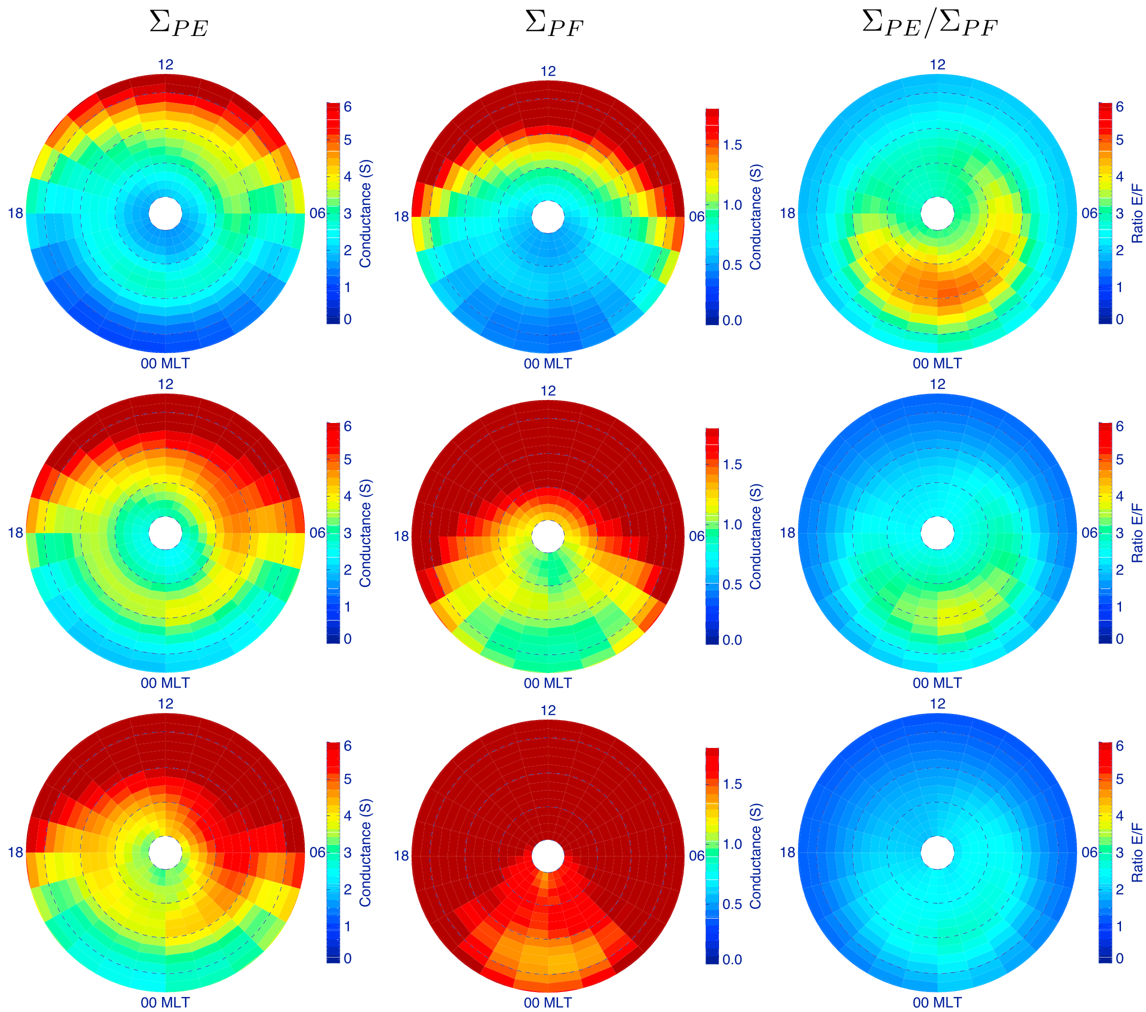

Figure 6. Same as Figure 5 but in the Southern Hemisphere.

auroral region in all three categories. With increasing solar flux, the ratio actually decreases. Although only observations under geomagnetically quiet conditions are used, it is still possible that the particle precipitation changes at certain level with the solar activity. Based on the DMSP particle measurements from 1984 to 1995, *Newell et al.* [1998] reported that the occurring frequency of intense aurora (>5 erg cm^{-2} s^{-1}) decreased with solar flux for sunlit conditions and was unaffected for dark conditions. Utilizing 13 years of electron data from the FAST satellite, *Cattell et al.* [2013] reached a similar conclusion for the sunlit conditions but found a negative correlation between the occurring frequency of intense aurora and solar flux. Meanwhile, *Zhou et al.* [2016] concluded that the aurora power in the nightside aurora oval under dark conditions decreased linearly with solar flux under geomagnetically quiet conditions ($Kp = 1-3$), by combing observations from TIMED/Global Ultraviolet Imager and DMSP/Special Sensor Ultraviolet Spectrographic Imager from 2002 to 2014. Therefore, both solar and aurora activities contribute to the decreasing trend of the ratio with solar flux. More detailed discussions have been included in the following paragraphs.

Figure 6 shows the variations of Σ_{PE}, Σ_{PF}, and γ_P with solar radiation in the Southern Hemisphere. Again, the two hemispheres share very similar features. But the influence of solar radiation on Σ_{PE} and Σ_{PF} is stronger in the Southern Hemisphere since the magnetic South Pole locates at a lower geographical latitude, which means the magnetic South Pole receives more sunlit than the magnetic North Pole in average. Both Σ_{PE} and Σ_{PF} in the Southern Hemisphere are larger than that in the Northern Hemisphere. Meanwhile, the ratio in the Southern Hemisphere is slightly smaller than that in the Northern Hemisphere since the ratio decreases with stronger solar radiation.

10.1002/2016SW001486

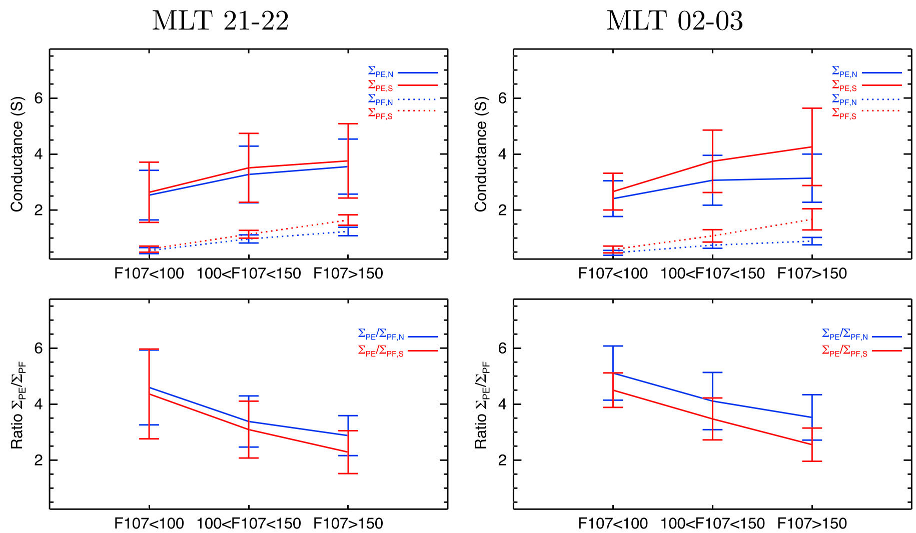

Figure 7. Comparisons of Σ_{PE}, Σ_{PF}, and their ratio (Σ_{PE}/Σ_{PF}) between the two hemispheres at (left column) MLT = 21–22 and (right column) MLT = 02–03 under different levels of solar radiation. Error bars represent standard deviation.

Interhemispheric asymmetry has been investigated in a number of studies and identified in different ionospheric and thermospheric parameters, e.g., hemispheric power [*Luan et al.*, 2010; *Zheng et al.*, 2013], ion convection pattern [*Lu et al.*, 1994; *Lukianova et al.*, 2008; *Pettigrew et al.*, 2010], and neutral density responses to geomagnetic storms [*Ridley et al.*, 2012]. In *Sheng et al.* [2014], an interhemispheric asymmetry that the seasonal variation of the ratio between Σ_{PE} and Σ_{PF} is larger in the Southern Hemisphere than in the Northern Hemisphere has been recognized. In this paper we further examine the interhemispheric asymmetry and focus on the local time dependence. Similar to the procedure in section 3.1, the dependence of Σ_{PE}, Σ_{PF}, and γ_P on the $F_{10.7}$ index at the center of the nighttime auroral zone (where Σ_{PE} maximizes) has been compared between the two hemispheres at two different local times, 02–03 MLT and 21–22 MLT, as shown in Figure 7. Interestingly, the difference of the ratio between the two hemispheres is again larger in the postmidnight sector than in the premidnight sector. First of all, solar radiation is not equal between the auroral zones in the two hemispheres due to the tilt and shift of the geomagnetic poles. The auroral activity is not symmetric between the two hemispheres as well [*Luan et al.*, 2010; *Laundal and Østgaard*, 2009]. Furthermore, even in the same hemisphere solar radiation and auroral activity are not evenly distributed between the premidnight and postmidnight sectors in the auroral zone. While the solar radiation is evenly distributed along geographical longitudes, the geomagnetic activity and auroral zone are oriented according to the geomagnetic coordinates, which were used to bin the data. As mentioned in the last section, the discrete aurora is found to peak in the premidnight sector and the diffuse aurora distributes from the premidnight to early morning hours [*Newell et al.*, 2009]. Additionally, the responses of the auroral power under dark conditions to solar activity have been found to be different between premidnight and postmidnight sectors [*Zhou et al.*, 2016]. All these factors may contribute to the local time dependence of the ratio and the interhemispheric asymmetry identified in this study. While the mean value of the ratio shows a modest difference in the postmidnight sector between the two hemispheres as discussed above, it has also been noticed that the differences are within the error bars, which indicate strong variations of the ionospheric conductivity in the nighttime auroral zone.

Geomagnetic activity and solar radiation control the conductance at high latitudes in different ways. Σ_{PE} increases with geomagnetic activity significantly, due to intensified auroral precipitation. Σ_{PF} also increases due to the stronger ionization at *F* region altitudes by auroral precipitation and plasma transport. Meanwhile, a positive correlation has been found between solar flux and ionospheric conductances (Σ_{PE} and Σ_{PF}) from Figures 5 and 6. However, the ratio between Σ_{PE} and Σ_{PF} generally increases with the *Ap* index but decreases with the $F_{10.7}$ index. This is related to the altitudinal distribution of energy associated with geomagnetic activity and solar radiation. Ionization caused by auroral particle precipitation (∼ keV) usually maximizes in the *E* region, while the ionization due to solar radiation peaks around 150 km [*Knipp et al.*, 2004, and references therein]. Therefore, with increasing *Ap* index, the enhancement in Σ_{PE} is relatively larger than that in Σ_{PF}, which results in a larger ratio. The situation is opposite with increasing $F_{10.7}$ index, the enhancement in Σ_{PF} is relatively larger and leads to a smaller ratio.

Altitudinal distributions of the Pedersen conductivity and energy deposition by Joule heating are crucial to accurate modeling of the neutral density response [e.g., *Deng et al.*, 2013]. In *Sheng et al.* [2014], the ratio between Σ_{PE} and Σ_{PF} derived from COSMIC EDPs was found to be smaller than those from TIEGCM simulations in the auroral zone, which indicates that the energy deposited in the *F* region may be underestimated in TIEGCM simulations. In this paper, the ratio is found to change with *Ap* and $F_{10.7}$ indices, which implies that the altitudinal distribution of energy deposition may also vary under different solar and geomagnetic conditions. These findings will help to quantify the altitudinal distribution of energy deposition in general circulation models and improve the simulations of neutral density variation.

4. Summary

COSMIC observations from 2009 to 2014 have been used to estimate the height-integrated Pedersen conductivity in the *E* (100–150 km) and *F* (150–600 km) regions. *Ap* and $F_{10.7}$ dependencies of Σ_{PE}, Σ_{PF}, and their ratio γ_P have been examined. Both Σ_{PE} and Σ_{PF} increase with the *Ap* and $F_{10.7}$ indices. Their ratio peaks in the postmidnight sector and increases with the *Ap* index but decreases with the $F_{10.7}$ index. It is also found that the conductance (both Σ_{PE} and Σ_{PF}) in the Southern Hemisphere is slightly larger than that in the Northern Hemisphere, since the south magnetic pole receives more sunlit. The difference of the ratio between the two hemispheres in the postmidnight sector is found to be larger than that in the premidnight sector. The possible mechanisms for the interhemispheric asymmetry in ionospheric conductance and their ratio include unequal energy inputs between the two hemispheres and uneven solar radiation and auroral activity between the premidnight and postmidnight sectors in the auroral zone. Further studies are needed to help fully understand the asymmetry.

Acknowledgments
This work was supported at UT Arlington by NSF through grant ATM 0955629 and AFOSR through award FA9550-16-1-0059 and MURI FA9559-16-1-0364. Xinan Yue would like to acknowledge the support by the Thousand Young Talents Program of China. The COSMIC data used in this study can be accessed from http://cdaac-www.cosmic.ucar.edu/cdaac/products.html. We acknowledge the use of NASA/GSFC's OMNIWeb service, which provided the $F_{10.7}$ and *Ap* indices.

References

Anthes, R. A., P. A. Berhardt, Y. Chen, L. Cucurull, K. F. Dymond, D. Ector, S. B. Healy, S. P. Ho, D. C. Hunt, and Y. H. Kuo (2008), The COSMIC/FORMOSAT-3 mission, *Bull. Am. Meteorol. Soc*, *89*, 313–333.

Brekke, A., J. R. Doupnik, and P. M. Banks (1974), Incoherent scatter measurements of e region conductivities and currents in the auroral zone, *J. Geophys. Res.*, *79*(25), 3773–3790.

Buonsanto, M. J. (1999), Ionospheric storms—A review, *Space Sci. Rev.*, *88*, 563–601, doi:10.1023/A:1005107532631.

Burns, A. G., Z. Zeng, W. Wang, J. Lei, S. C. Solomon, A. D. Richmond, T. L. Killeen, and Y. H. Kuo (2008), Behavior of the F_2 peak ionosphere over the South Pacific at dusk during quiet summer conditions from COSMIC data, *J. Geophys. Res.*, *113*, A12305, doi:10.1029/2008JA013308.

Cattell, C., J. Dombeck, and L. Hanson (2013), Solar cycle effects on parallel electric field acceleration of auroral electron beams, *J. Geophys. Res. Space Physics*, *118*, 5673–5680, doi:10.1002/jgra.50546.

Danilov, A., and J. Lastovicka (2001), Effects of geomagnetic storms on the ionosphere and atmosphere, *Int. J. Geomag. Aeron.*, *2*(3), 209–224.

Deng, Y., T. J. Fuller-Rowell, A. J. Ridley, D. Knipp, and R. E. Lopez (2013), Theoretical study: Influence of different energy sources on the cusp neutral density enhancement, *J. Geophys. Res. Space Physics*, *118*, 2340–2349, doi:10.1002/jgra.50197.

Evans, D. S., N. C. Maynard, J. Trøim, T. Jacobsen, and A. Egeland (1977), Auroral vector electric field and particle comparisons, 2. Electrodynamics of an arc, *J. Geophys. Res.*, *82*(16), 2235–2249.

Fang, X., C. E. Randall, D. Lummerzheim, S. C. Solomon, M. J. Mills, D. R. Marsh, C. H. Jackman, W. Wang, and G. Lu (2008), Electron impact ionization: A new parameterization for 100 eV to 1 MeV electrons, *J. Geophys. Res.*, *113*, A09311, doi:10.1029/2008JA013384.

Fuller-Rowell, T. J., and D. S. Evans (1987), Height-integrated Pedersen and Hall conductivity patterns inferred from the TIROS-NOAA satellite data, *J. Geophys. Res.*, *92*(A7), 7606–7618.

Hajj, G., L. Lee, X. Pi, L. Romans, W. Schreiner, P. Straus, and C. Wang (2000), Cosmic GPS ionospheric sensing and space weather, *Terr. Atmos. Oceanic Sci.*, *11*(1), 235–272.

Hardy, D. A., M. S. Gussenhoven, R. Raistrick, and W. J. McNeil (1987), Statistical and functional representations of the pattern of auroral energy flux, number flux, and conductivity, *J. Geophys. Res.*, *92*(A11), 12,275–12,294.

He, M., L. Liu, W. Wan, B. Ning, B. Zhao, J. Wen, X. Yue, and H. Le (2009), A study of the Weddell Sea Anomaly observed by FORMOSAT-3/COSMIC, *J. Geophys. Res.*, *114*, A12309, doi:10.1029/2009JA014175.

Kaeppler, S., D. Hampton, M. Nicolls, A. Strømme, S. Solomon, J. Hecht, and M. Conde (2015), An investigation comparing ground-based techniques that quantify auroral electron flux and conductance, *J. Geophys. Res. Space Physics*, *120*, 9038–9056, doi:10.1002/2015JA021396.

Knipp, D. J., W. K. Tobiska, and B. A. Emery (2004), Direct and indirect thermospheric heating sources for solar cycles 21–23, *Sol. Phys.*, *224*, 495–505, doi:10.1007/s11207-005-6393-4.

Laundal, K. M., and N. Østgaard (2009), Asymmetric auroral intensities in the Earth's Northern and Southern Hemispheres, *Nature*, *460*(7254), 491–493.

Lei, J., S. Syndergaard, A. G. Burns, S. C. Solomon, W. Wang, Z. Zeng, R. G. Roble, Q. Wu, Y. H. Kuo, and J. M. Holt (2007), Comparison of COSMIC ionospheric measurements with ground-based observations and model predictions: Preliminary results, *J. Geophys. Res.*, *112*, A07308, doi:10.1029/2006JA012240.

Lu, G., et al. (1994), Interhemispheric asymmetry of the high-latitude ionospheric convection pattern, *J. Geophys. Res.*, *99*(A4), 6491–6510.

Luan, X., W. Wang, A. Burns, S. C. Solomon, and J. Lei (2008), Midlatitude nighttime enhancement in *F* region electron density from global COSMIC measurements under solar minimum winter condition, *J. Geophys. Res.*, *113*, A09319, doi:10.1029/2008JA013063.

Luan, X., W. Wang, A. Burns, S. Solomon, Y. Zhang, and L. J. Paxton (2010), Seasonal and hemispheric variations of the total auroral precipitation energy flux from TIMED/GUVI, *J. Geophys. Res.*, *115*, A11304, doi:10.1029/2009JA015063.

Lukianova, R., C. Hanuise, and F. Christiansen (2008), Asymmetric distribution of the ionospheric electric potential in the opposite hemispheres as inferred from the SuperDARN observations and FAC-based convection model, *J. Atmos. Sol. Terr. Phys.*, *70*(18), 2324–2335.

McGranaghan, R., D. J. Knipp, T. Matsuo, H. Godinez, R. J. Redmon, S. C. Solomon, and S. K. Morley (2015), Modes of high-latitude auroral conductance variability derived from DMSP energetic electron precipitation observations: Empirical orthogonal function analysis, *J. Geophys. Res. Space Physics*, *120*, 11,013–11,031, doi:10.1002/2015JA021828.

McGranaghan, R., D. J. Knipp, T. Matsuo, and E. Cousins (2016), Optimal interpolation analysis of high-latitude ionospheric Hall and Pedersen conductivities: Application to assimilative ionospheric electrodynamics reconstruction, *J. Geophys. Res. Space Physics*, *121*, 4898–4923, doi:10.1002/2016JA022486.

Millward, G. H., R. J. Moffett, H. F. Balmforth, and A. S. Rodger (1999), Modeling the ionospheric effects of ion and electron precipitation in the cusp, *J. Geophys. Res.*, *104*, 24,603–24,612, doi:10.1029/1999JA900249.

Moen, J., and A. Brekke (1990), On the importance of ion composition to conductivities in the auroral ionosphere, *J. Geophys. Res.*, *95*, 10,687–10,693, doi:10.1029/JA095iA07p10687.

Moen, J., and A. Brekke (1993), The solar flux influence on quiet time conductances in the auroral ionosphere, *Geophys. Res. Lett.*, *20*(10), 971–974.

Moldwin, M. (2008), *An Introduction to Space Weather*, Cambridge Univ. Press, Cambridge, U. K.

Newell, P. T., C.-I. Meng, and S. Wing (1998), Relation to solar activity of intense aurorae in sunlight and darkness, *Nature*, *393*(6683), 342–344.

Newell, P. T., T. Sotirelis, and S. Wing (2009), Diffuse, monoenergetic, and broadband aurora: The global precipitation budget, *J. Geophys. Res.*, *114*, A09207, doi:10.1029/2009JA014326.

Pedatella, N. M., H.-L. Liu, F. Sassi, J. Lei, J. L. Chau, and X. Zhang (2014), Ionosphere variability during the 2009 SSW: Influence of the lunar semidiurnal tide and mechanisms producing electron density variability, *J. Geophys. Res. Space Physics*, *119*, 3828–3843, doi:10.1002/2014JA019849.

Pedatella, N. M., X. Yue, and W. S. Schreiner (2015), An improved inversion for FORMOSAT-3/COSMIC ionosphere electron density profiles, *J. Geophys. Res. Space Physics*, *120*, 8942–8953, doi:10.1002/2015JA021704.

Pettigrew, E., S. Shepherd, and J. Ruohoniemi (2010), Climatological patterns of high-latitude convection in the Northern and Southern Hemispheres: Dipole tilt dependencies and interhemispheric comparisons, *J. Geophys. Res.*, *115*, A07305, doi:10.1029/2009JA014956.

Rasmussen, C. E., R. W. Schunk, and V. B. Wickwar (1988), A photochemical equilibrium model for ionospheric conductivity, *J. Geophys. Res.*, *93*(A9), 9831–9840.

Richmond, A. D., and G. Lu (2000), Upper-atmospheric effects of magnetic storms: A brief tutorial, *J. Atmos. Sol. Terr. Phys.*, *62*, 1115–1127, doi:10.1016/S1364-6826(00)00094-8.

Ridley, A. J., D. Zhang, and Z. Xiao (2012), Analyzing the hemispheric asymmetry in the thermospheric density response to geomagnetic storms, *J. Geophys. Res.*, *117*, A08317, doi:10.1029/2011JA017259.

Robinson, R. M., and R. R. Vondrak (1984), Measurements of *E* region ionization and conductivity produced by solar illumination at high latitudes, *J. Geophys. Res.*, *89*(A6), 3951–3956.

Robinson, R. M., R. R. Vondrak, K. Miller, T. Dabbs, and D. Hardy (1987), On calculating ionospheric conductances from the flux and energy of precipitating electrons, *J. Geophys. Res.*, *92*, 2565–2569, doi:10.1029/JA092iA03p02565.

Rocken, C., K. Ying-Hwa, W. S. Schreiner, D. Hunt, S. Sokolovskiy, and C. McCormick (2000), COSMIC system description, *Terr. Atmos. Oceanic Sci.*, *11*(1), 21–52.

Scherer, K., H. Fichtner, B. Heber, and U. Mall (2005), *Space Weather: The Physics Behind a Slogan*, Springer, Berlin.

Schreiner, W., C. Rocken, S. Sokolovskiy, S. Syndergaard, and D. Hunt (2007), Estimates of the precision of GPS radio occultations from the COSMIC/FORMOSAT-3 mission, *Geophys. Res. Lett.*, *34*, L04808, doi:10.1029/2006GL027557.

Sheng, C., Y. Deng, X. Yue, and Y. Huang (2014), Height-integrated Pedersen conductivity in both *E* and *F* regions from COSMIC observations, *J. Atmos. Sol. Terr. Phys.*, *115*, 79–86, doi:10.1016/j.jastp.2013.12.013.

Spiro, R. W., P. H. Reiff, and L. J. Maher Jr. (1982), Precipitating electron energy flux and auroral zone conductances—An empirical model, *J. Geophys. Res.*, *87*, 8215–8227, doi:10.1029/JA087iA10p08215.

Strangeway, R. J. (2012), The equivalence of Joule dissipation and frictional heating in the collisional ionosphere, *J. Geophys. Res.*, *117*, A02310, doi:10.1029/2011JA017302.

Thayer, J. P., J. F. Vickrey, R. A. Heelis, and J. B. Gary (1995), Interpretation and modeling of the high-latitude electromagnetic energy flux, *J. Geophys. Res.*, *100*(A10), 19,715–19,728.

Vickrey, J. F., R. R. Vondrak, and S. J. Matthews (1981), The diurnal and latitudinal variation of auroral zone ionospheric conductivity, *86*(A1), 65–75, doi:10.1029/JA086iA01p00065.

Wu, B. H., V. Chu, P. Chen, and T. Ting (2005), FORMOSAT-3/COSMIC science mission update, *GPS Solutions*, *9*(2), 111–121.

Yue, X., W. S. Schreiner, J. Lei, C. Rocken, Y. H. Kuo, and W. Wan (2010a), Climatology of ionospheric upper transition height derived from COSMIC satellites during the solar minimum of 2008, *J. Atmos. Sol. Terr. Phys.*, *72*(17), 1270–1274.

Yue, X., W. S. Schreiner, J. Lei, C. Rocken, D. C. Hunt, Y. H. Kuo, and W. Wan (2010b), Global ionospheric response observed by COSMIC satellites during the January 2009 stratospheric sudden warming event, *J. Geophys. Res.*, *115*, A00G09, doi:10.1029/2010JA015466.

Yue, X., W. S. Schreiner, C. Rocken, Y. H. Kuo, and J. Lei (2012), Artificial ionospheric wave number 4 structure below the F_2 region due to the Abel retrieval of radio occultation measurements, *GPS Solutions*, *16*, 1–7.

Yue, X., W. S. Schreiner, Y.-H. Kuo, Q. Wu, Y. Deng, and W. Wang (2013), GNSS radio occultation (RO) derived electron density quality in high latitude and polar region: NCAR-TIEGCM simulation and real data evaluation, *J. Atmos. Sol. Terr. Phys.*, *98*, 39–49, doi:10.1016/j.jastp.2013.03.009.

Zeng, Z., A. Burns, W. Wang, J. Lei, S. Solomon, S. Syndergaard, L. Qian, and Y.-H. Kuo (2008), Ionospheric annual asymmetry observed by the COSMIC radio occultation measurements and simulated by the TIEGCM, *J. Geophys. Res.*, *113*, A07305, doi:10.1029/2007JA012897.

Zheng, L., S. Fu, Q. Zong, G. Parks, C. Wang, and X. Chen (2013), Solar cycle dependence of the seasonal variation of auroral hemispheric power, *Chin. Sci. Bull.*, *58*(4–5), 525–530.

Zhou, S., X. Luan, and X. Dou (2016), Solar activity dependence of nightside aurora in winter conditions, *J. Geophys. Res. Space Physics*, *121*, 1619–1626, doi:10.1002/2015JA021865.